

## Rational approximations in the parabolic equation method for water waves

JAMES T. KIRBY

*Coastal and Oceanographic Engineering Department, University of Florida, Gainesville, FL 32611, U.S.A.*

(Received November 12, 1985; revised and accepted April 28, 1986)

### ABSTRACT

Kirby, J.T., 1986. Rational approximations in the parabolic equation method for water waves. *Coastal Eng.*, 10: 355-378.

Approximations based on minimax principles are developed in order to allow for large-angle propagation in the parabolic equation method. Numerical studies show that the minimax approximations do not cause any significant degradation of accuracy at small angles of incidence when compared with an existing model based on a (1,1) Padé approximant, and that they allow for much more successful treatment of large angles of incidence than is possible using the previously available methods.

### 1. INTRODUCTION

The application of the parabolic equation method (PEM) to any relevant wave propagation problem implies that a principal propagation direction may be identified in the  $\{x,y\}$  plane of propagation. Then, an aperture, or window of directions with respect to the principal direction, is associated with any particular approximation, and limits the range of propagation directions which may be adequately represented by the approximation (Fig. 1). The borders of a given aperture are defined only loosely and depend mainly on the amount of error the modeller is willing to allow in the wave prediction. This error may be evaluated for any given approximation by examining the approximation in terms of the related expansion of the wavenumber vector. Errors in predicted wavelengths and propagation directions may then be evaluated directly.

The purpose of this paper is to develop a set of parabolic approximations based on a minimax principle, which have the effect of maximizing the allowed aperture  $\theta_a$  within arbitrarily chosen limits of error introduced in approximations for small  $\theta$ . In section 2, we first review existing parabolic approximations and their connection to Padé approximants relating the components of

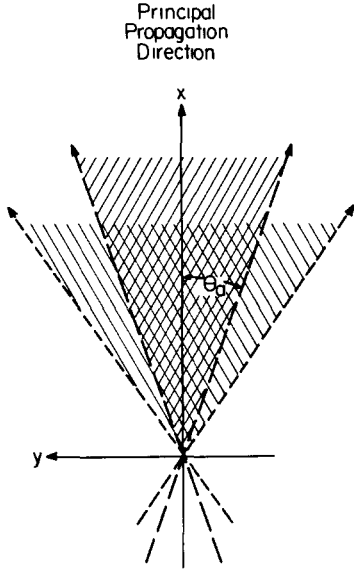


Fig. 1. Definition of aperture for parabolic approximations: // // // allowed aperture: lower-order approximation; \\ \\ \\ \\ allowed aperture: higher-order approximation.

the wavenumber vector. Then in section 3, we discuss methods for obtaining higher-order approximations based alternatively on minimax approximations, and present the resulting numerical coefficients. In section 4, we develop the appropriate PEM for weakly nonlinear waves on slowly varying water depth. Several computational examples are considered in section 5, and it is shown that the minimax approximations developed here are successful in allowing relatively large angles of wave propagation in the computational grid. We conclude with a discussion of approximations which are tailored to a specific angle of incidence in the computational grid.

2. PARABOLIC EQUATIONS AND PADÉ APPROXIMANTS

The lowest-order parabolic equation for forward scattering of time-harmonic linear waves in the  $x$  (principal) direction in water of constant depth may be derived by substituting:

$$\eta(x,y) = A(x,y) e^{i(kx - \omega t)} \tag{2.1}$$

into the governing Helmholtz equation:

$$\nabla_h^2 \eta + k^2 \eta = 0 \tag{2.2}$$

to obtain:

$$2ikA_x + A_{yy} = 0 + \text{higher-order terms} \tag{2.3}$$

where we have assumed:

$$|A_x| \ll O(k|A|) \quad (2.4)$$

This approximation may be examined in light of the plane wave of permanent form:

$$\eta = ae^{i(lx + my - \omega t)}; \quad l^2 + m^2 = k^2 \quad (2.5)$$

$A(x, y)$  in eqn. (2.1) is then given by:

$$A(x, y) = ae^{i[(l-k)x + my]} \quad (2.6)$$

which gives:

$$\frac{l}{k} = 1 - \frac{1}{2} \left( \frac{m}{k} \right)^2 \quad (2.7)$$

after substitution in eqn. (2.3). Equation (2.7) in turn is the lowest-order binomial expansion (or, equivalently, the (1,0) Padé approximant) of:

$$\frac{l}{k} = \left\{ 1 - \left( \frac{m}{k} \right)^2 \right\}^{1/2} \quad (2.8)$$

for fixed  $m/k = \sin \theta \ll 1$ ,  $\theta$  being the propagation direction. The accuracy of any approximation over the range of propagation directions  $0 \leq \theta \leq \theta_a$ , where  $\theta_a$  is the aperture width, may be evaluated by comparing predicted  $l/k$  to exact  $l/k = \cos \theta$  over the range in question. This comparison is given in Fig. 2 for eqn (2.7). Equation (2.7) forms the basis of the lowest-order approximations

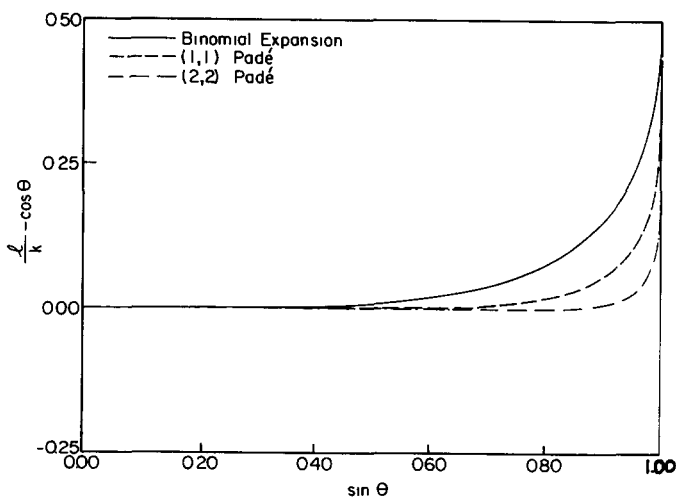


Fig. 2. Absolute errors  $(l/k) - \cos \theta$  for several expansions of  $(l/k) = [1 - (m/k)^2]^{1/2}$  about  $(m/k) \rightarrow 0$ . — binomial expansion; - - - (1,1) Padé approximant; - · - (2,2) Padé approximant.

given by Radder (1979) for water waves and Tappert (1977) for underwater sound propagation.

One of the simplest ways of extending the accuracy of a polynomial expansion is to construct a rational approximation consisting of the ratio of two polynomial expressions. Of the possible choices, the Padé approximant serves as the logical starting point (Baker, 1975). For eqn. (2.8), the appropriate (1,1) Padé approximant is given by:

$$\frac{l}{k} = \frac{1 - \frac{3}{4} \left(\frac{m}{k}\right)^2}{1 - \frac{1}{4} \left(\frac{m}{k}\right)^2} \quad (2.9)$$

The Padé approximant has the property of predicting the proper value and slope of the approximated function  $l/k$  as  $m/k$  (or  $\theta$ ) becomes small. The approximation thus maintains the accuracy of the lowest-order approximation at small  $\theta$ , and at the same time extends the accuracy of the approximation as  $\theta$  increases, as shown in Fig. 2. Rewriting eqn. (2.9) as:

$$2k(l-k) + m^2 - \frac{1}{2}(l-k)m^2 = 0 \quad (2.10)$$

and retracing the steps of eqns. (2.3)–(2.6) using the method of operator correspondence then gives:

$$2ikA_x + A_{yy} + \frac{i}{2k} A_{xyy} = 0 \quad (2.11)$$

Dingemans (1983) and Kirby (1986a) have shown that the no-current, constant-depth form of Booij's (1981) parabolic approximation is essentially equivalent to eqn. (2.11), and proposed the Padé approximant as the relevant analysis of the splitting method employed by Booij to obtain his PEM approximation. Kirby (1986a) has further shown, by means of multiple-scale expansion to the proper order, that the correct evolution equation to the next higher order beyond that giving eqn. (2.3) is given by:

$$2ikA_x + A_{yy} + \frac{k}{C_g} \frac{\partial C_g}{\partial k} A_{xx} - \frac{ik}{C_g} \frac{\partial}{\partial k} \left(\frac{C_g}{k}\right) A_{xyy} - \frac{1}{4C_g} \frac{\partial}{\partial k} \left(\frac{C_g}{k}\right) A_{yyy} = 0 \quad (2.12)$$

in which eqn. (2.3) represents the lowest-order terms. Using eqn. (2.3) to eliminate terms in  $A_{xx}$  and  $A_{yyy}$  in favor of terms in  $A_{xyy}$  reduces eqn. (2.12) to eqn. (2.11). Interestingly, using the same substitutions to eliminate terms in  $A_{xyy}$  and  $A_{yyy}$  in favor of  $A_{xx}$  terms reduces eqn. (2.12) to the elliptic form:

$$2ikA_x + A_{yy} + A_{xx} = 0 \quad (2.13)$$

which is the exact governing equation in the present context. The (1,1) Padé

form of the PEM thus has at least a reasonable connection to the theory of higher-order approximations, within allowable limits of substitution between higher-order terms using lower-order results. Similar approximations applied to underwater sound propagation are described by Botseas et al. (1983).

The multiple-scale method used by Kirby (1986a), or the Padé approximant itself, can in principle be extended to any higher-order degree; in particular, the next relevant Padé approximant would be the (2,2) approximant:

$$\frac{l}{k} = \frac{1 - \frac{5}{4} \left(\frac{m}{k}\right)^2 + \frac{5}{16} \left(\frac{m}{k}\right)^4}{1 - \frac{3}{4} \left(\frac{m}{k}\right)^2 + \frac{1}{16} \left(\frac{m}{k}\right)^4} \quad (2.14)$$

which is presented in Fig. 2. The desirability of carrying approximations to this order is apparent. However, all approximations at this order would involve derivative terms of higher order than  $A_x$ ,  $A_{yy}$  or  $A_{xy}$  and are then not resolvable by the Crank-Nicolson implicit algorithm (and resulting tridiagonal matrix) usually applied to parabolic equations.

### 3. MINIMAX APPROXIMATION

Greene (1984, 1985) has suggested that improvements may be achieved while staying within the scheme of eqn. (2.9) by relaxing the exact connection between eqn. (2.9) and eqn. (2.8) as  $(m/k) \rightarrow 0$  in favor of adopting an approximation which minimizes the maximum error  $(l/k - \cos \theta)$  over a prespecified aperture  $0 \leq \theta \leq \theta_a$ . Greene investigated these so-called minimax approximations, which may be written in the present context as:

$$\frac{l}{k} = \frac{a_0 + a_1 \left(\frac{m}{k}\right)^2}{1 + b_1 \left(\frac{m}{k}\right)^2} \quad (3.1)$$

for values of  $\theta_a$  up to  $40^\circ$ . It is suspected that Greene did not extend the calculations to higher values of  $\theta_a$  due to the increasing degradation of accuracy in the limit  $\theta \rightarrow 0$ , as will be discussed below. Since Greene's results are presented in different form and since he considers a maximum  $\theta_a$  of only  $40^\circ$ , it is relevant to reinvestigate approximations of the form (3.1). To do so, we have performed the determination of the minimax approximation (3.1) which minimizes the error:

$$e = \text{MAX} |l/k(\theta) - \cos \theta|; \quad 0 \leq \theta \leq \theta_a \quad (3.2)$$

where  $l/k$  is predicted by eqn. (3.1) and  $\cos \theta = l/k$  is given by eqn. (2.8). The procedure for obtaining minimax approximations is too extensive to summarize here; the reader is referred, for example, to Chapter 6 of Morris (1983). Calculations here were performed using the Harwell library subroutine PEØ5AD (Hopper, 1979). A list of values of  $a_0$ ,  $a_1$  and  $b_1$  for (3.1) are given in Table 1 for aperture widths ranging from 10 to 90° in increments of 10°. The coefficient values are seen to be asymptotic to the (1,1) Padé approximant as  $\theta_a \rightarrow 0$ . Figure 3 gives plots of the absolute error in predicted ( $l/k$ ) for values of  $\theta_a = 40^\circ$ ,  $60^\circ$  and  $80^\circ$ . A plot of the (1,1) Padé approximant, eqn. (2.9), is

TABLE 1

Coefficients of the rational approximation determined by varying aperture width

Aperture	$a_0$	$a_1$	$b_1$
Padé	1	-0.75	-0.25
10°	0.999999972	-0.752858477	-0.252874920
20°	0.999998178	-0.761464683	-0.261734267
30°	0.999978391	-0.775898646	-0.277321130
40°	0.999871128	-0.796244743	-0.301017258
50°	0.999465861	-0.822482968	-0.335107575
60°	0.998213736	-0.854229482	-0.383283081
70°	0.994733030	-0.890064831	-0.451640568
80°	0.985273164	-0.925464479	-0.550974375
90°	0.956311082	-0.943396628	-0.704401903

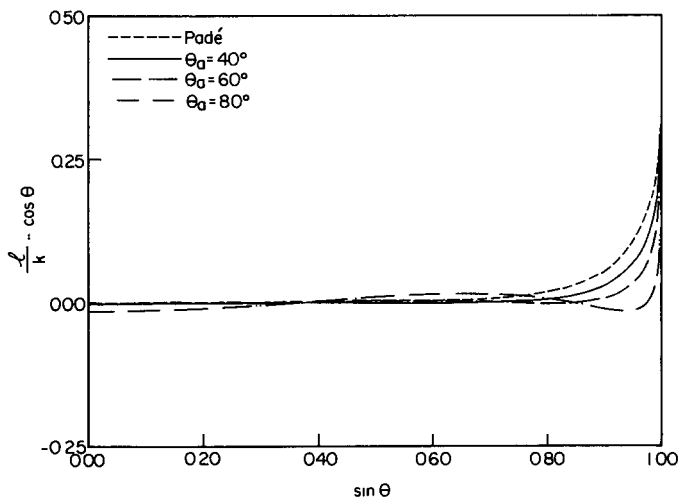


Fig. 3. Absolute errors  $(l/k) - \cos \theta$  for various aperture widths  $\theta_a$  for the minimax (1,1) rational approximation. - - -  $\theta_a = 0^\circ$  (Padé); —  $\theta_a = 40^\circ$ ; - · -  $\theta_a = 60^\circ$ ; - - -  $\theta_a = 80^\circ$ .

included for comparison. For values of  $\theta_a \leq 60^\circ$ , the correspondence between the minimax and (1,1) Padé approximant remains close at  $\theta = 0$ , the deviation for  $\theta_a = 60^\circ$  being  $(1 - a_0) \times 100 = 0.2\%$ . Deviations for  $\theta_a > 60^\circ$  at  $\theta = 0$  increase rapidly due to the difficulty in approximating eqn. (2.8) as  $m/k \rightarrow 1$ . However, the advantages of the  $\theta_a = 60^\circ$  approximation over the (1,1) Padé approximant, when considered over the entire range  $0 \leq m/k \leq 1$ , are apparent. A comparison of Figs. 2 and 3 indicates that the  $\theta_a = 60^\circ$  approximation attains about the same level of accuracy as  $m/k \rightarrow 1$  as the (2,2) Padé approximant, with only a slight decrease in accuracy at small values of  $\theta$ .

Using the method of operator correspondence to back-track again, eqn. (3.1) may be used to derive the corresponding parabolic approximation:

$$2ikA_x + 2k^2(a_0 - 1)A + 2(b_1 - a_1)A_{yy} - \frac{2ib_1}{k}A_{xyy} = 0 \quad (3.3)$$

which reduces to eqn. (2.11) as  $\theta_a \rightarrow \theta$ . Looking at the case of  $\theta = 0$  ( $\partial/\partial y = 0$ ), we see that:

$$A_x = ik(a_0 - 1)A \quad (3.4)$$

giving a wave of the form:

$$\eta = ae^{ik a_0 x} \quad (3.5)$$

with wavelength:

$$L_{\theta_a} = \frac{2\pi}{ka_0} = L(\text{exact}) \times a_0^{-1} > L(\text{exact}) \quad (3.6)$$

The effect of the deviation of the value of  $a_0$  from 1, and hence  $(l/k)(\theta = 0)$  from  $\cos(0) = 1$ , is to distort the wavelength of a wave propagating in the principal propagation direction. Since range (or distance over an accumulated number of wavelengths) is a quantity of major interest in the underwater sound application, this distortion may be the factor causing Greene to limit his aperture widths to  $40^\circ$ . However, in surface-water wave applications, problem areas are at present confined to a relatively small number of wavelengths, while the possible presence of strong refraction effects leads to the desirability of utilizing the larger-aperture approximations developed here.

As a means of further comparing the various approximations, values of numerically predicted normalized wavenumber:

$$k' = \left[ \left( \frac{l}{k} \right)^2 + \left( \frac{m}{k} \right)^2 \right]^{1/2} \quad (3.7)$$

and numerically predicted propagation direction calculated by:

$$\theta_N = \tan^{-1} \left\{ \left( \frac{m}{k} \right) / \left( \frac{l}{k} \right) \right\} \quad (3.8)$$

are given in Table 2 for three choices of  $\theta_a$ . An inspection of the results in Table 2 suggests that an aperture of  $\theta_a = 70^\circ$ , with a corresponding wavelength distortion of 0.6% at  $\theta = 0$ , may be a reasonable approximation in most present applications of the PEM.

TABLE 2

Numerically predicted wavenumbers and propagation directions for several empirical approximations

$\theta$ ( $^\circ$ )	$\frac{l}{k}$ (exact)	$\frac{l}{k}$ (numerical)	$k'$ (eqn. 3.7)	$\theta_N$ ( $^\circ$ ) (eqn. 3.8)
$\theta_a = 0^\circ$ ( <i>Padé</i> ):				
0	1	1	1	0
10	0.984808	0.984809	1.000002	10.0000
20	0.939692	0.939749	1.000106	19.9989
30	0.866025	0.866667	1.000555	29.9816
40	0.766044	0.769615	1.002738	39.8689
50	0.642788	0.656142	1.008636	49.4189
60	0.5	0.538462	1.019775	58.1282
70	0.342020	0.433411	1.034827	65.2396
80	0.173648	0.359870	1.048500	69.9266
90	0	0.333333	1.111111	71.5651
$\theta_a = 60^\circ$ :				
0	1	0.998214	0.998214	0
10	0.984808	0.983826	0.999033	10.0098
20	0.939692	0.940454	1.000715	19.9851
30	0.866025	0.867811	1.001546	29.9489
40	0.766044	0.766681	1.000486	39.9766
50	0.642788	0.641125	0.998939	50.0726
60	0.5	0.501786	1.000894	59.9114
70	0.342020	0.368694	1.009434	68.5772
80	0.173648	0.270172	1.021195	74.6589
90	0	0.233469	1.026892	76.8586
$\theta_a = 70^\circ$ :				
0	1	0.994733	0.994733	0
10	0.984808	0.981258	0.996504	10.0354
20	0.939692	0.940293	1.000564	19.9882
30	0.866025	0.870506	1.003883	29.8721
40	0.766044	0.770820	1.003663	39.8248
50	0.642788	0.642780	0.999995	50.0003
60	0.5	0.494782	0.997401	60.2596
70	0.342020	0.347287	1.001814	69.7169
80	0.173648	0.234007	1.012228	76.6334
90	0	0.190875	1.018054	79.1936

#### 4. THE PARABOLIC APPROXIMATION FOR WEAKLY NONLINEAR WAVES ON SLOWLY VARYING DEPTH AND CURRENT

We are now in a position to extend the PEM approximation to waves in a slowly varying domain by employing the correspondences between existing PEM approximations and the formulae derived above. Kirby (1986a) gave a parabolic approximation for forward-scattered, weakly nonlinear Stokes waves in water with slowly varying depth and ambient current, which may be written in the form:

$$\frac{\partial}{\partial x} \left\{ k^{1/2} (p - U^2)^{1/2} \left( 1 + \frac{P_1 M}{k^2 (p - U^2)} \right) \right\} \tilde{\phi}^+ = i k k^{1/2} (p - U^2)^{1/2} \left( 1 + \frac{P_2 M}{k^2 (p - U^2)} \right) \tilde{\phi}^+ \quad (4.1)$$

where  $\tilde{\phi}^+$  is related to the wave velocity potential  $\phi$  by:

$$\phi(x, y, z, t) = \tilde{\phi}^+(x, y) \frac{\cosh k(h+z)}{\cosh kh} e^{-i\omega t} \quad (4.2)$$

with:

$$\omega = \sigma + \underline{k}(x, y) \cdot \underline{U}(x, y)$$

$$\sigma = (gk \tanh kh)^{1/2} \quad (4.3)$$

and where:

$$M\tilde{\phi}^+ = \{2\omega k U + i\omega(\nabla_h \cdot \underline{U}) - \sigma^2 k^2 D|A|^2 + i\sigma w\} \tilde{\phi}^+ - (UV\tilde{\phi}_y^+)_x - (UV\tilde{\phi}_x^+)_y + [(p - V^2)\tilde{\phi}_y^+]_y + 2i\omega \underline{U} \cdot \nabla_h \tilde{\phi}^+ \quad (4.4)$$

and:

$$p = CC_g, \quad C = \sigma/k, \quad C_g = \partial\sigma/\partial k$$

The coefficients  $P_1$  and  $P_2$  are given by:

$$P_1 = 0; \quad P_2 = 1/2 \quad (4.5a)$$

or:

$$P_1 = 1/4; \quad P_2 = 3/4 \quad (4.5b)$$

The two sets of coefficients  $(P_1, P_2)$  are related to the lowest-order binomial expansion (2.7) and the (1,1) Padé approximant (2.9), respectively. Following this line of reasoning, we switch from the approximation (2.9) to the min-imax approximation (3.1) and introduce the coefficients  $a_0, a_1, b_1$  in eqn. (4.1) according to:

$$\frac{\partial}{\partial x} \left\{ k^{1/2} (p - U^2)^{1/2} \left( 1 - \frac{b_1 M}{k^2 (p - U^2)} \right) \right\} \tilde{\phi}^+ = i k k^{1/2} (p - U^2)^{1/2} \left( a_0 - \frac{a_1 M}{k^2 (p - U^2)} \right) \tilde{\phi}^+ \quad (4.6)$$

To date, the model has only been tested in the absence of currents due to lack of available data. For this case,  $M\tilde{\phi}^+$  reduces to:

$$M\tilde{\phi}^+ = (CC_g \tilde{\phi}_y^+)_y + i\omega w \tilde{\phi}^+ - \omega^2 k^2 D |A|^2 \tilde{\phi}^+ \quad (4.7)$$

The second and third terms on the right-hand side of eqn. (4.7) represent the effects of dissipation (with  $w$  generally a complex dissipation coefficient) and third-order nonlinear self-interaction, respectively, with:

$$D = (\cosh 4kh - 8 + 2 \tanh^2 kh) / 8 \sinh^4 kh$$

Substituting:

$$\tilde{\phi}^+ = A e^{i \int \bar{k}(x) dx} \quad (4.8)$$

where  $\bar{k}(x)$  is some average of  $k(x,y)$  over the  $y$ -direction and where we assume that wave phase accumulates principally in the  $x$ -direction, leads to the parabolic equation:

$$C_g A_x + i(\bar{k} - a_0 k) C_g A + \frac{1}{2} (C_g)_x A + \frac{i}{\omega} \left( a_1 - b_1 \frac{\bar{k}}{k} \right) (CC_g A_y)_y - \frac{b_1}{\omega k} (CC_g A_y)_{yx} + \frac{b_1}{\omega} \left( \frac{k_x}{k^2} + \frac{(C_g)_x}{2k C_g} \right) (CC_g A_y)_y + \frac{i\omega k^2}{2} D |A|^2 A + \frac{w}{2} A = 0 \quad (4.9)$$

where we have arbitrarily retained the correct form (in the sense of a multiple scale expansion) of the nonlinear and dissipation terms. Equation (4.9) may be written in finite-difference form using the Crank-Nicolson formulation. The scheme is extended to include higher-order derivatives by writing the term  $(CC_g A_y)_{yx}$  as:

$$\begin{aligned} (CC_g A_y)_{yx} \Big|_{\substack{x=(i+\frac{1}{2})\Delta x \\ y=j\Delta y}} &= \left\{ [(CC_{g_{i+1}}^{i+1} + CC_{g_i}^{i+1})(A_{j+1}^{i+1} - A_j^{i+1}) \right. \\ &\quad - (CC_{g_i}^{i+1} + CC_{g_{i-1}}^{i+1})(A_j^{i+1} - A_{j-1}^{i+1})] / 2\Delta y^2 \\ &\quad \left. - [(CC_{g_{i+1}}^i + CC_{g_i}^i)(A_{j+1}^i - A_j^i) - (CC_{g_i}^i + CC_{g_{i-1}}^i) \right. \\ &\quad \left. (A_j^i - A_{j-1}^i)] / 2\Delta y^2 \right\} / \Delta x \end{aligned} \quad (4.10)$$

This formulation fits conveniently in the usual tridiagonal matrix formulation

of the Crank-Nicolson implicit scheme. For the case of constant coefficients and no nonlinearity or dissipation, stability analysis shows that the resulting scheme is unconditionally stable with an amplification factor  $|A^{i+1}/A^i| = 1$ . The finite-difference formulation for the usual parabolic portion of the equation may be found in Kirby and Dalrymple (1983).

## 5. MODEL PERFORMANCE AT SMALL AND LARGE ANGLES OF PROPAGATION

Before testing the large-angle capabilities of the present model, it is necessary to show that the relaxation of model accuracy at small angles of propagation does not cause a degradation of performance in comparison with previous models. For this purpose, we use the laboratory results of Berkhoff et al. (1982), who studied the focusing of waves by a submerged elliptic shoal resting on a plane beach. This data set has been extensively employed as a test of parabolic model accuracy. Kirby and Dalrymple (1984) have shown that the lowest-order parabolic approximation provides a good model of wave focusing in this experiment when nonlinear effects are included. More recently, Kirby (1986a) has shown that additional features of the amplitude envelope such as the diffraction fringes are well predicted using a model incorporating the (1,1) Padé approximant and the approximate nonlinear model of Kirby and Dalrymple (1986). We thus assume that the results of the (1,1) Padé approximant model may be used as a reference case, against which the minimax approximations may be tested for loss of accuracy as errors at small angles of incidence are allowed to increase. The topography and measurement transects are shown in

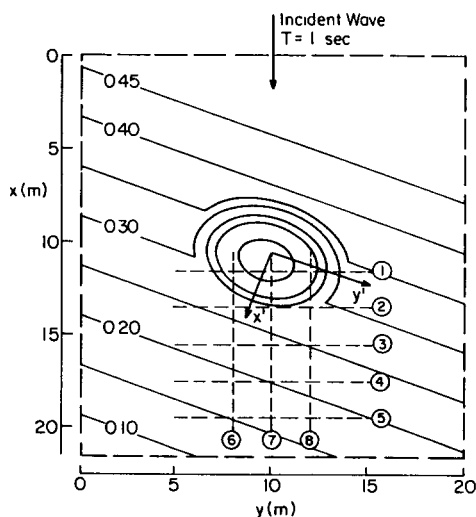
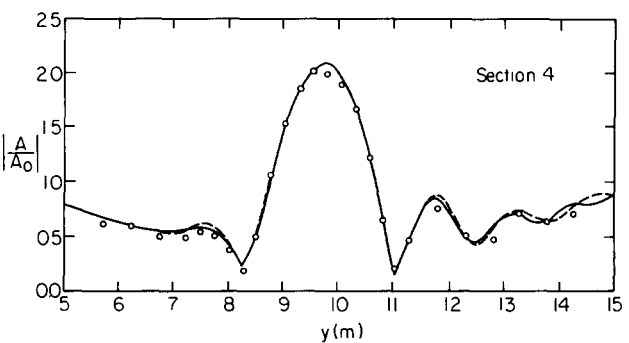
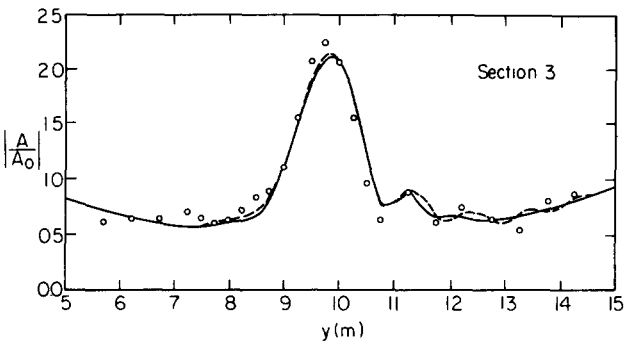
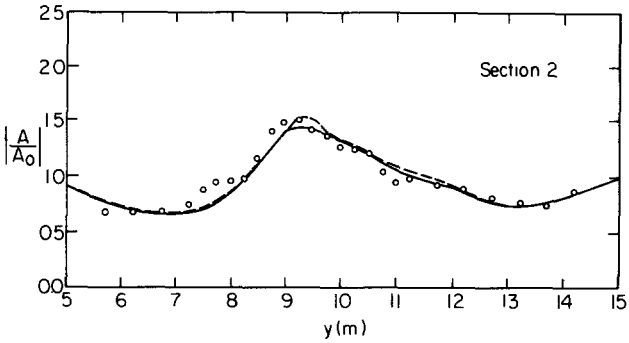
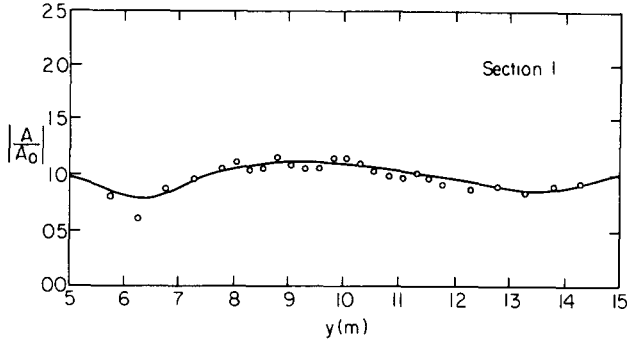


Fig. 4. Experimental configuration: Berkhoff et al. (1982). Labeled transects correspond to section 1 through 8 in Figs. 5 and 6.



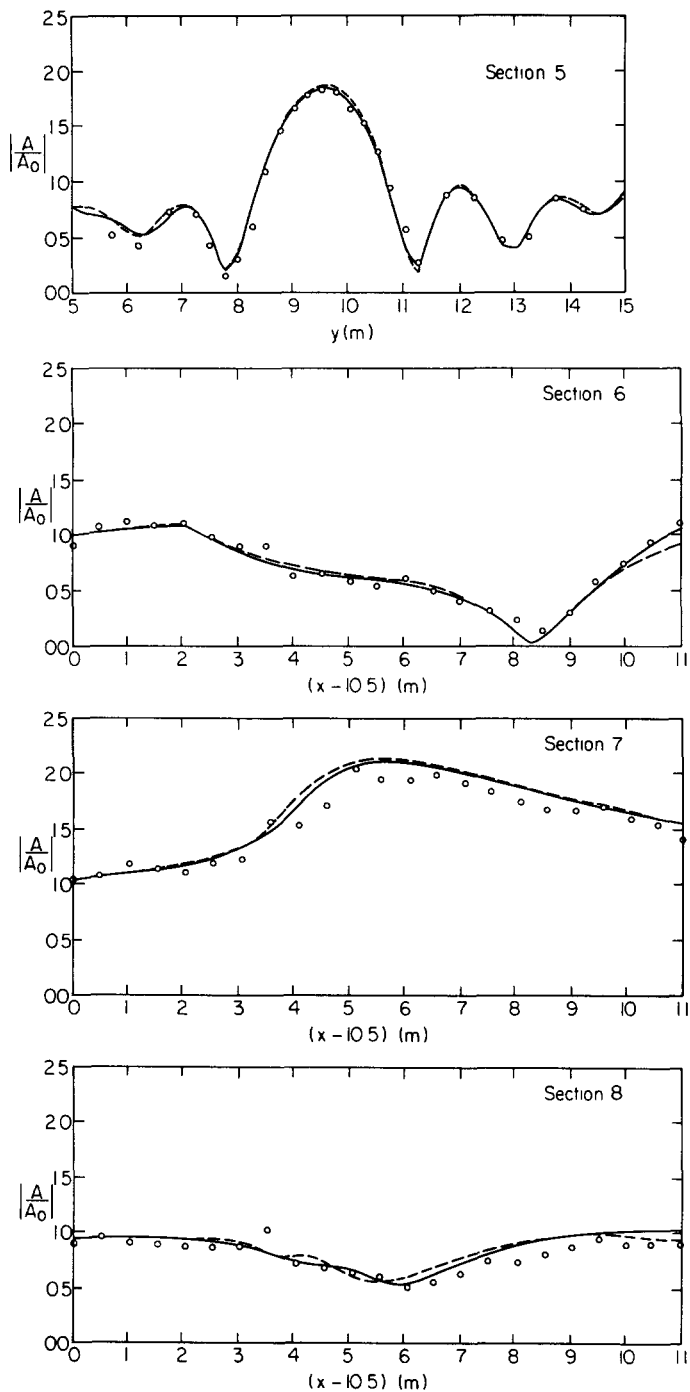
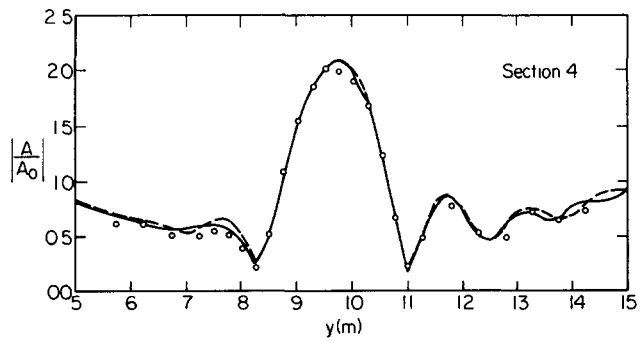
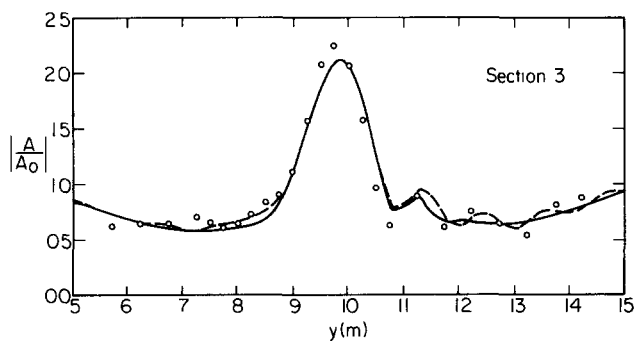
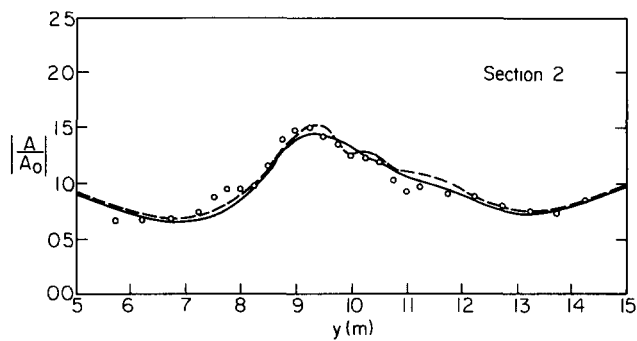
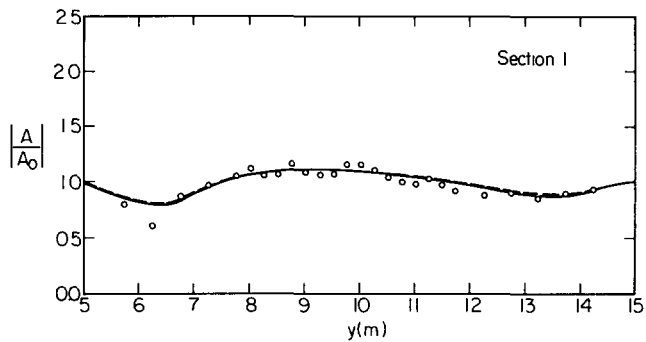


Fig. 5. Comparison of minimax approximation ( $\theta_a = 60^\circ$ ) with (1,1) Padé approximant (Kirby, 1986a) and laboratory data (Berkhoff et al., 1982). — Padé; - - -  $\theta_a = 60^\circ$ ; 0 data.



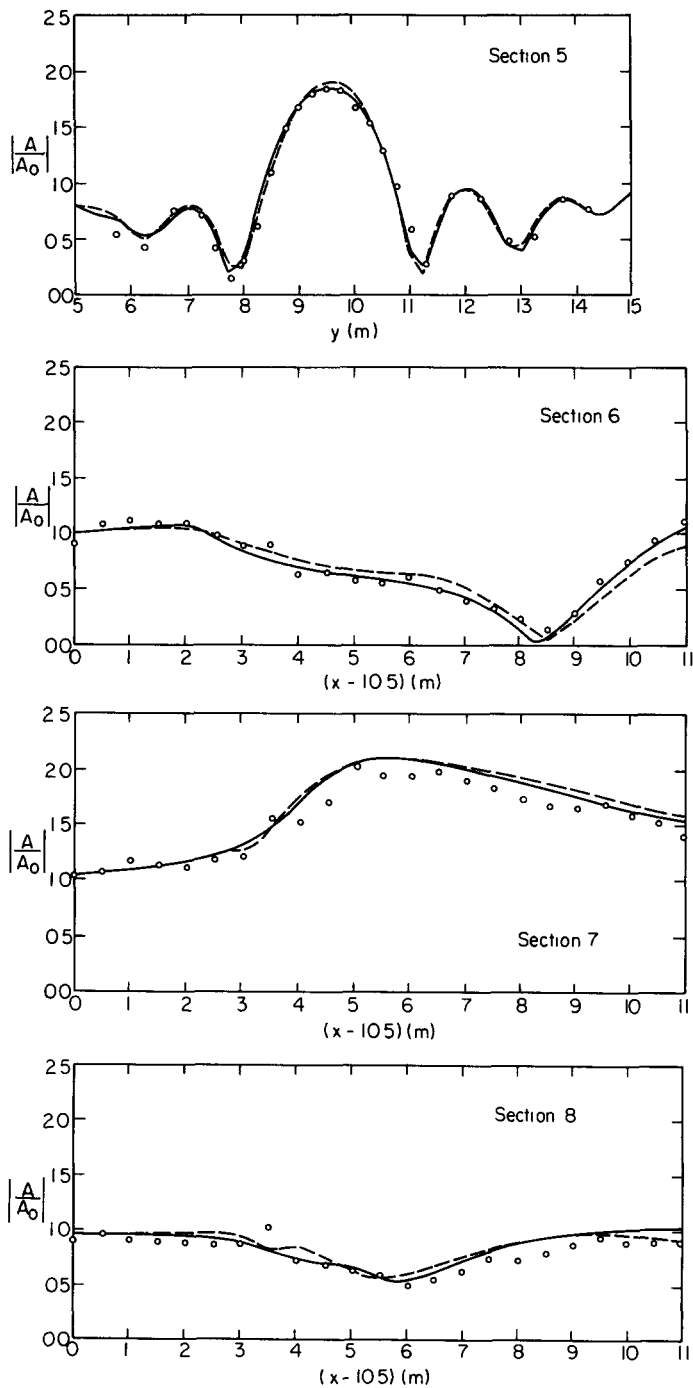


Fig. 6. Comparison of minimax approximation ( $\theta_a=70^\circ$ ) with (1,1) Padé approximant (Kirby, 1986a) and laboratory data (Berkhoff et al., 1982). — Padé; - - -  $\theta_a=70^\circ$ ; 0 data.

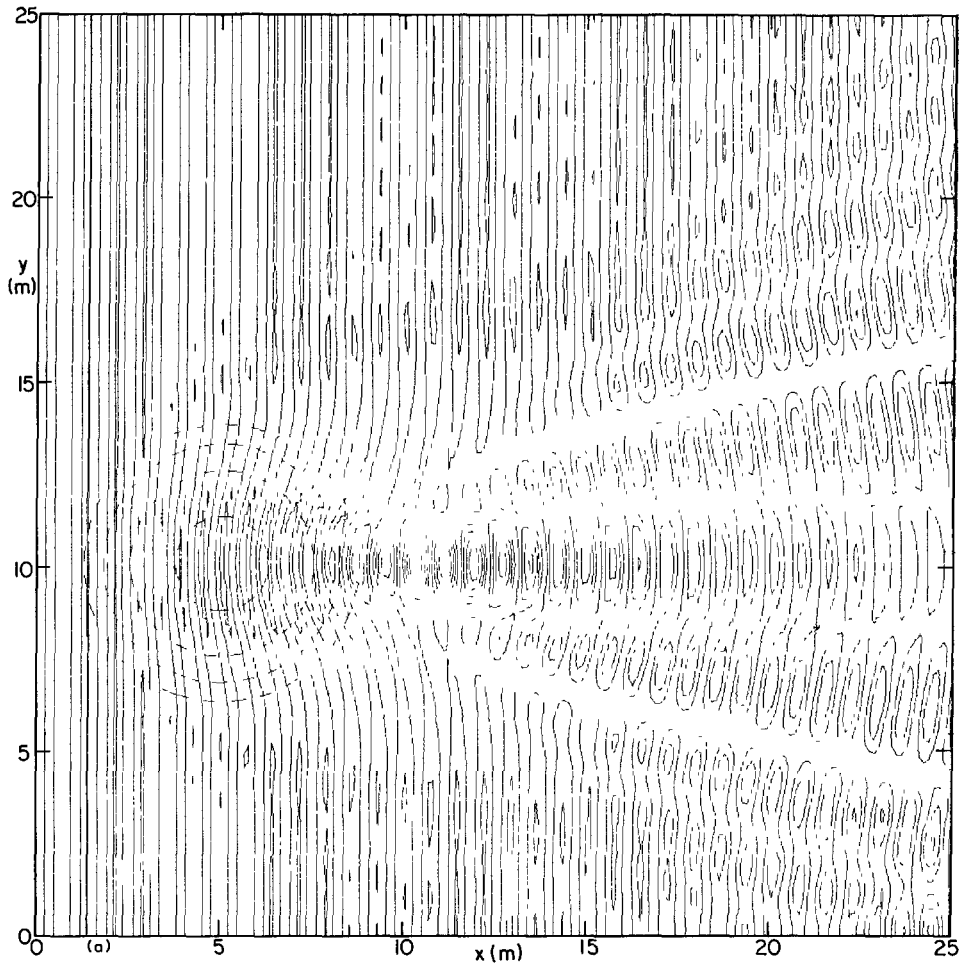


Fig. 4; reference may be made to Kirby (1986a) and Berkhoff et al. (1982) for a description of the topography.

Two tests were conducted in order to determine the amount of degradation of accuracy in the large-aperture models. Aperture angles of  $60^\circ$  and  $70^\circ$  were chosen, as this represents the range where error at normal incidence starts to become significant. Results for the  $60^\circ$  and  $70^\circ$  aperture approximations are plotted for the labelled transects 1–8 in Figs. 5 and 6, respectively. All calculations were performed using a wave period  $T = 1$  s, wave amplitude  $A_0 = 0.0232$  m, and a uniform grid spacing  $\Delta x = \Delta y = 0.25$  m.

An inspection of Figs. 5 and 6 indicates that each minimax approximation deviates (to varying degree) from the prediction of the Padé model. Differences between the  $60^\circ$  aperture model and the Padé model (Fig. 5) seem to be localized and non-systematic, except for a slightly faster focusing of waves in

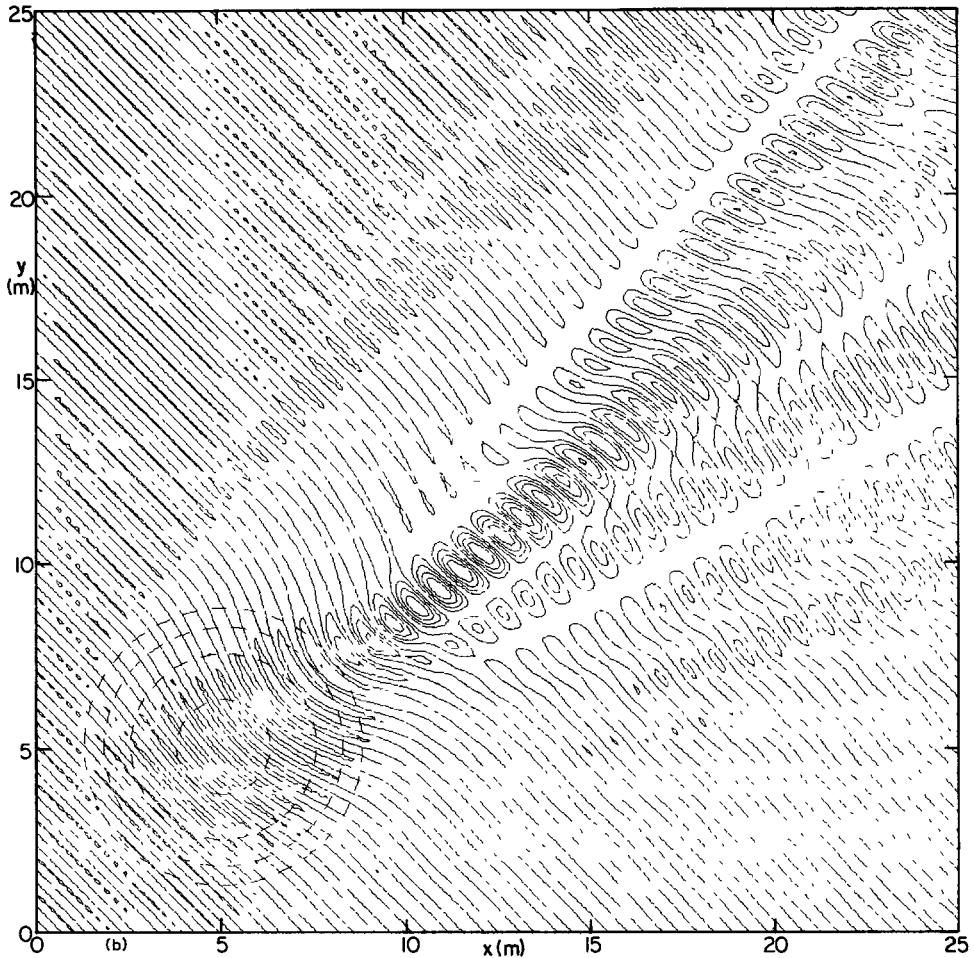


Fig. 7. Wave fields calculated using the (1,1) Padé model. Contours are in increments of  $0.5 A_0$  for instantaneous  $\eta(x,y)$ . (a)  $\theta_0=0^\circ$ , normal incidence. (b)  $\theta_0=45^\circ$ .

the  $60^\circ$  model. Overall, the  $60^\circ$  model corresponds well to the Padé model, and both are good models of the laboratory data.

The  $70^\circ$  aperture model also is a good predictor of the overall structure of the focus and wave field. However, the small deviations from the Padé results seem to take on a more systematic character here, especially with regard to a slight overprediction of the focus height which increases with downwave distance (Fig. 6, section 7) and a downwave-displacement of a partial node of the amplitude envelope on section 6. This general downwave displacement of features may be due to the accumulated effect of the overprediction of wavelength in the  $70^\circ$  model.

Strictly speaking, the  $60^\circ$  model corresponds better to the experimental

results and previous calculations than does the  $70^\circ$  model, and therefore seems to be a better choice for situations where the principal angle is essentially normal to the grid but where spreading angle (diffraction or refraction effects) may be relatively large. However, deviation between data and the  $70^\circ$  model is not drastic or even terribly significant, and the  $70^\circ$  model would still be a suitable choice for most situations of this type.

A further run to test the  $80^\circ$  aperture model (for which the distortion to wavelength in the normal incidence direction is 1.5%) indicated an accentuation of the systematic distortion to the focusing pattern which begins to develop in the  $70^\circ$  approximation, with the deviations in the  $70^\circ$  approximation being increased by a factor of 2-3. In particular, the partial node apparent on transect 6 is displaced to a position close to  $(x-10.5)=9$  m, almost one meter from the Padé result. It appears that the  $70^\circ$  approximation represents some sort of relative upper bound for quantitative accuracy; the  $80^\circ$  approximation begins to exhibit only a qualitative agreement with data and other approximations.

Having verified that large-aperture approximations in the range of  $60-70^\circ$  represent good predictors of wave field development at small angles of incidence, we turn to the question of initial propagation at large angles to the pre-established computational grid. In order to maintain some correspondence with the previous example, we choose the case of a circular shoal with dimensions similar to the laboratory shoal of Berkhoff et al. (1982). We choose geometry:

$$h(x,y) = \begin{cases} h_0 = 0.336 \text{ m} & ; r > R \\ h_0 + 0.3 - 0.5 \left\{ 1 - \left[ \left( \frac{x}{5} \right)^2 + \left( \frac{y}{5} \right)^2 \right] \right\}^{1/2} & ; r \leq R \end{cases} \quad (5.1)$$

where  $R = 4$  m and  $r = (x^2 + y^2)^{1/2}$ . The symmetry of the shoal allows the incident wave field to be rotated to any angle to the  $x$ -axis; a "correct" model will be one that causes no distortion to the resulting focusing pattern resulting from changes in  $\theta_0$ , the incidence angle.

We take a rectangular grid with  $\Delta x' = \Delta y' = 0.25$  m and overall dimensions  $0 \leq x' y' \leq 24.75$  m. We use the incident wave period and amplitude conditions of Berkhoff et al. (1982). Two incident wave directions are studied;  $\theta_0 = 0^\circ$ , with the shoal centered at  $(x', y') = (5, 10)$ , and  $\theta_0 = 45^\circ$ , with the shoal centered at  $(x', y') = (5, 5)$ . Open lateral boundary conditions are applied using the algorithm given in Kirby (1986b).

For the first series of tests, we use the (1,1) Padé model of Kirby (1986a) to study the two incident wave angles. Figure 7 shows the wave patterns for the two incidence angles in the form of contours of surface elevation in increments of  $0.5 A_0$ . The asymmetrical distortion to the focusing pattern at the  $45^\circ$  angle of incidence is apparent, as is a tendency for the focus to be shifted off the picture diagonal in the  $+x$  direction, or downwave in the computational sense.

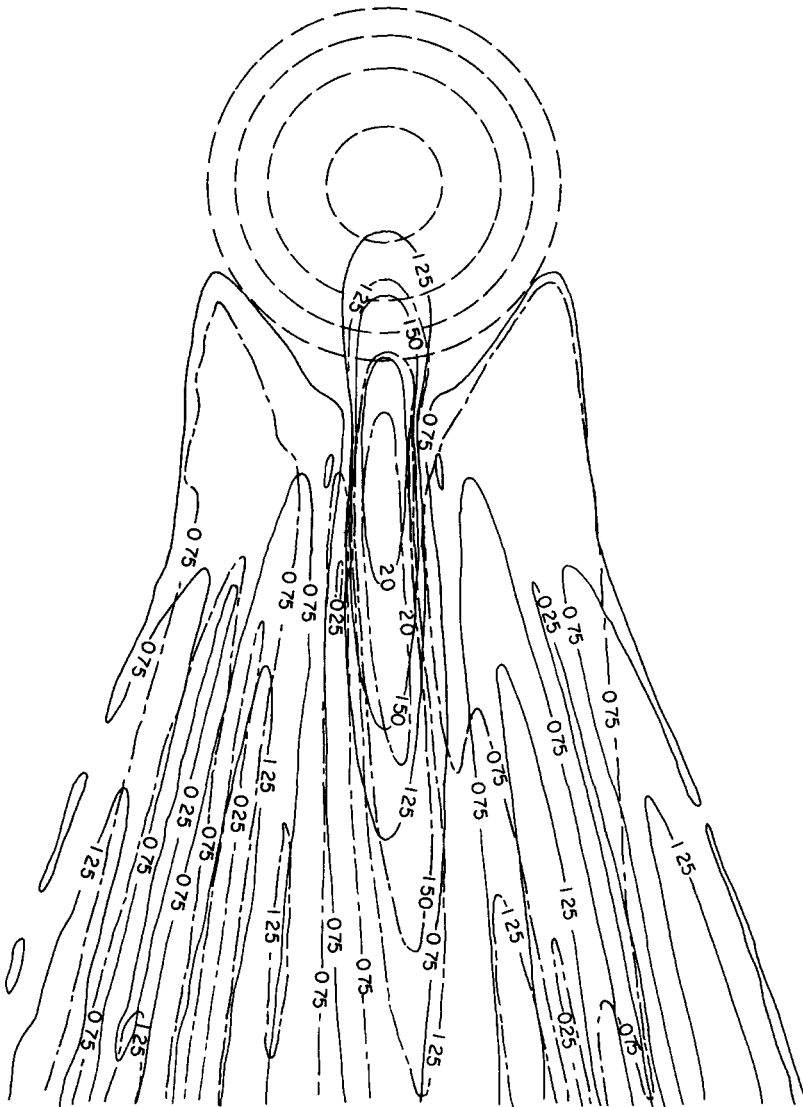


Fig. 8. Amplitude contours and topography for circular shoal. Amplitude contours  $|A/A_0|$  as labelled; (1,1) Padé approximant. —  $\theta_0=0^\circ$ ; - - -  $\theta_0=45^\circ$ ; - - - depth contours.

The distortion to the wave pattern due to the  $45^\circ$  angle of incidence is illustrated clearly by the superposition of wave amplitude contours in Fig. 8. The superposition was obtained by rotating the wave field of Fig. 7b about the center of the shoal by  $36.5^\circ$  in a counterclockwise sense, or  $45^\circ$  minus an  $8.5^\circ$  distortion which represents the angle between the diagonal and the line joining the shoal center to the point of maximum wave height in the focus. This  $8.5^\circ$

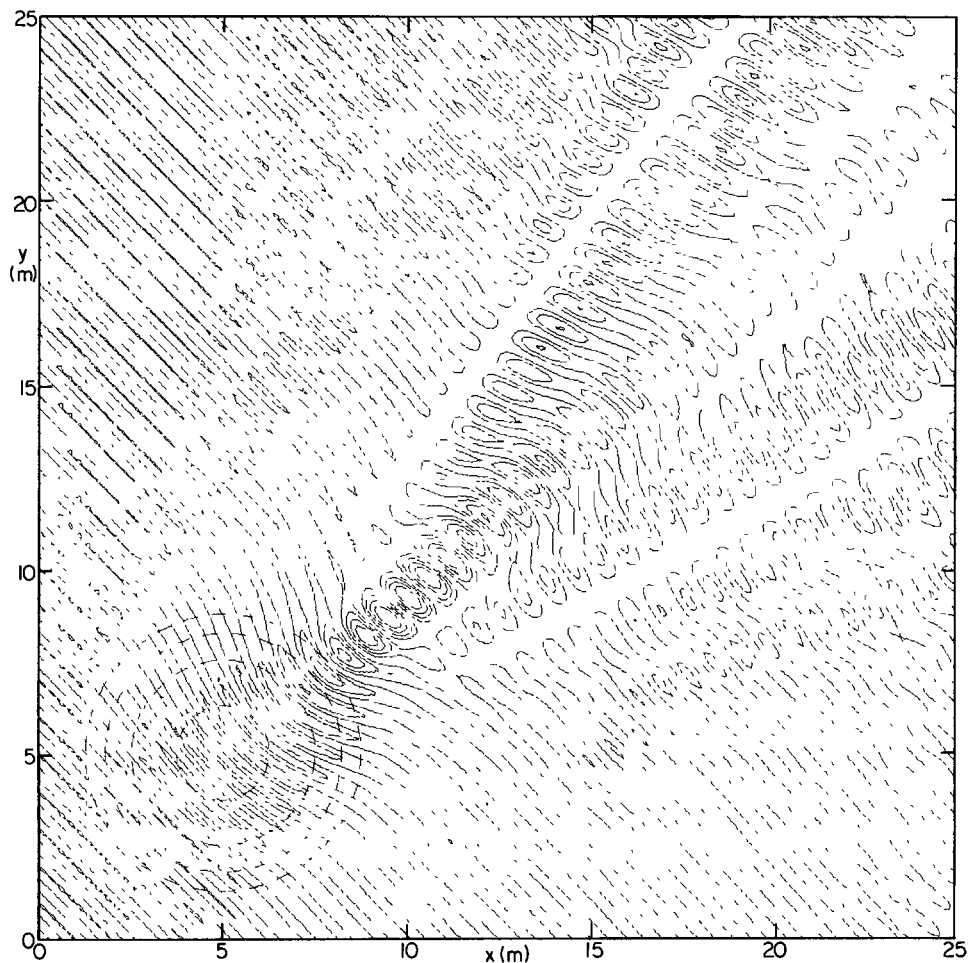


Fig. 9. Wave field calculated using  $\theta_a = 70^\circ$  model;  $\theta_0 = 45^\circ$ . Contours as in Fig. 7.

distortion accounts for the shift of the diffraction pattern in the downwave sense on the computation grid. Figure 8 shows clearly that the focus is elongated and shifted further from the shoal center than in the normal incidence case, with corresponding distortion in the diffraction fringes. Contour values in Fig. 8 (and Fig. 10) are relative to incident wave amplitude.

Figure 9 shows the wave field for the  $45^\circ$  angle of incidence, using the  $\theta_a = 70^\circ$  minimax approximation. There is still some apparent asymmetric distortion and a shift of the focus off the diagonal in the  $+x$  direction; however, these effects are much less accentuated than in the Padé model. Amplitude contours for the normal and  $45^\circ$  incidence in the  $70^\circ$  approximation are superposed in Fig. 10. Here the counterclockwise rotation of the  $45^\circ$  case is  $39.75^\circ$ , with a

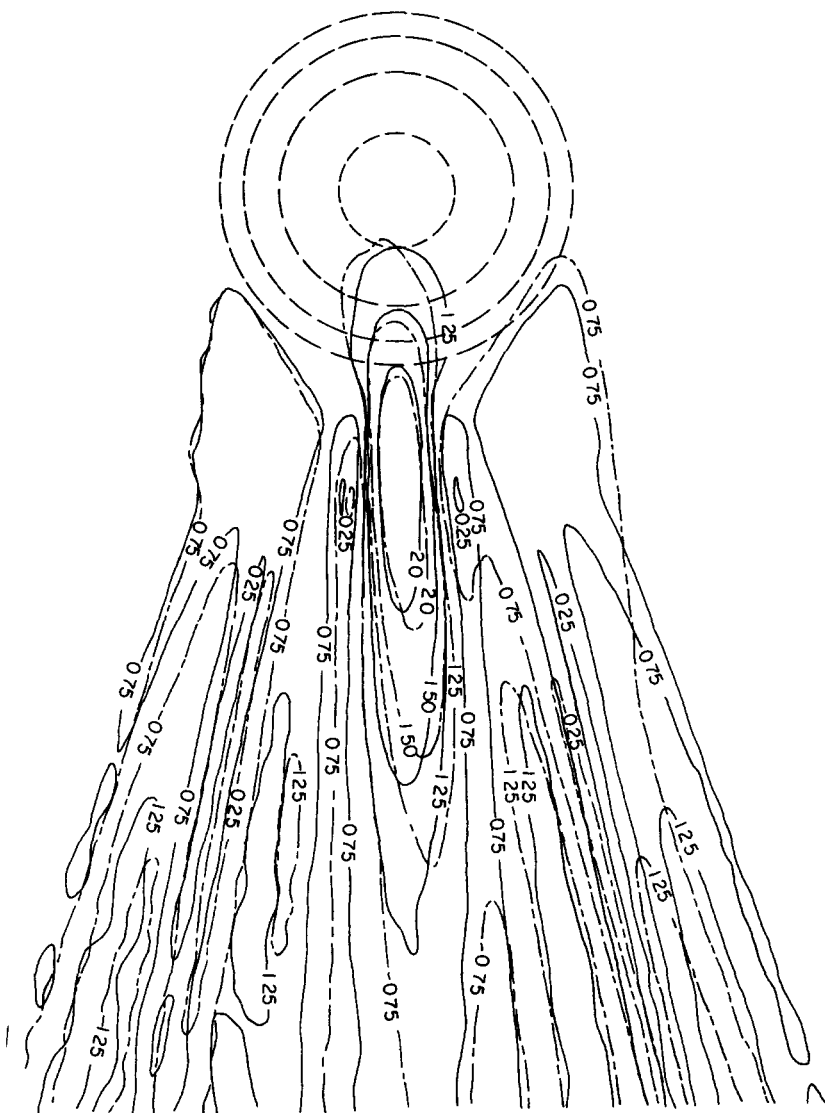


Fig. 10. Amplitude contours and topography for circular shoal  $\theta_a = 70^\circ$  approximation. —  $\theta_0 = 0^\circ$ ; - - -  $\theta_0 = 45^\circ$ ; - - - - depth contours.

distortion of  $5.25^\circ$ . The two results agree reasonably well in terms of the area and extent of contours in the focus, and in the distance of the focus from the shoal center. The overall diffraction pattern is maintained reasonably well out to two maxima of the diffraction fringe away from the central focus.

The  $\theta_a = 70^\circ$  minimax approximation clearly provides a better model for large-angle propagation than does the Padé approximant model of Kirby (1986a). Further tests were conducted using the  $80^\circ$  approximation. This model

exhibited marginally better agreement between  $\theta_0=0^\circ$  and  $45^\circ$  than did the  $70^\circ$  model, but caused a significant distortion to the overall extent of the focus in comparison to the Padé and  $70^\circ$  models.

6. DISCUSSION OF UN-CENTERED APERTURES

This study has shown that large-aperture minimax approximations can provide a significant extension of the range of validity of the PEM. Tests indicate that aperture widths on the order of  $\pm 70^\circ$  may be used with little short-range distortion to a wave field resulting from errors in predicted wavelength.

The freedom to choose a particular aperture also leads to the question of whether apertures centered on a nonzero principal angle could be constructed for cases where the non-zero angle is known in advance. For the examples above, this would lead to the consideration of apertures of the form  $45^\circ \pm \theta_a$ . Table 3 gives computed coefficients for apertures centered on  $45^\circ$ , with  $\theta_a$  ranging from  $10^\circ$  to  $40^\circ$ . Errors for these choices are shown in Fig. 11. It was

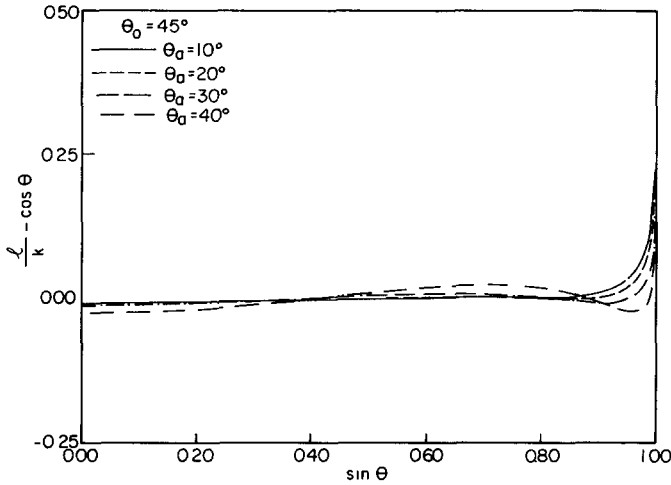


Fig. 11. Absolute errors  $(l/k) - \cos \theta$  for various aperture widths, for an aperture centered on  $\theta = 45^\circ$ . —  $\theta_a = 10^\circ$ ; - - -  $\theta_a = 20^\circ$ ; - · - ·  $\theta_a = 30^\circ$ ; - - - -  $\theta_a = 40^\circ$ .

TABLE 3

Coefficients of the rational approximation for varying aperture width, centered on  $\theta_0 = 45^\circ$

Aperture $\theta_a^\circ$	$a_0$	$a_1$	$b_1$
10	0.989725391	-0.855391072	-0.410525678
20	0.988862080	-0.875510773	-0.444238479
30	0.985955255	-0.906411468	-0.508501259
40	0.974025149	-0.938102389	-0.619921508

found that the form of the function  $\cos \theta$  as  $\theta \rightarrow 90^\circ$  did not allow these approximations to give significantly better approximations in the limit  $\theta \rightarrow 90^\circ$  without accruing significant error over the aperture width. The approximation  $45^\circ \pm 30^\circ$  was found to give suitable results for the circular shoal problem, but an inspection of the coefficients for this case shows that this approximation differs very little from the  $70^\circ$  aperture centered on  $0^\circ$ . It appears that, for examples such as those shown here, there is little advantage in choosing a specialized aperture over using a broad aperture centered around normal incidence.

## 7. CONCLUSIONS

It has been shown that the range of wave angles which is allowable within the limitations of the parabolic approximation may be significantly increased by relaxing the local accuracy of approximations based on Padé approximants at normal wave incidence in favor of minimax approximations, which minimize the maximum error occurring over a prespecified range of wave directions. Numerical results are given which show that the resulting minimax approximations do not cause significant distortion to calculated wavefields at small angles of incidence. Further, we have shown that the minimax approximations provide quantitatively accurate results for a focusing pattern developing in a wave propagating at  $45^\circ$  to the principal direction. This range of quantitative accuracy is seen to be well beyond the limitations of the (1,1) Padé approximant model given earlier by Kirby (1986a).

## REFERENCES

- Baker, G.A., 1975. *Essentials of Padé Approximants*. Academic Press.
- Berkhoff, J.C.W., Booij, N. and Radder, A.C., 1982. Verification of numerical wave propagation models for simple harmonic linear waves. *Coastal Eng.*, 6: 255-279.
- Booij, N., 1981. Gravity waves on water with non-uniform depth and current. Report 81-1, Dept. of Civil Eng., Delft Univ. of Technology.
- Botseas, G., Gilbert, K.E. and Lee, D., 1983. IFD: wide angle capability. NUSC Tech. Rept. 6905, Naval Underwater Systems Center, New London, Conn.
- Dingemans, M.W., 1983. Verification of numerical wave propagation models with field measurements: CREDIZ verification Haringvliet. Report W488 part 1, Delft Hydraulics Laboratory.
- Greene, R.R., 1984. The rational approximation to the acoustic wave equation with bottom interaction. *J. Acoust. Soc. Am.*, 76: 1764-1733.
- Greene, R.R., 1985. A high-angle one-way wave equation for seismic wave propagation along rough and sloping interfaces. *J. Acoust. Soc. Am.*, 77: 1991-1998.
- Hopper, M.J., 1979. Harwell subroutine library; a catalogue of subroutines. Report AERE-R9185, United Kingdom Atomic Energy Authority.
- Kirby, J.T., 1986a. Higher-order approximations in the parabolic equation method for water waves. *J. Geophys. Res.*, 91: 933-952.

- Kirby, J.T., 1986b. Open lateral boundary condition for application in the parabolic equation method. *J. Waterway, Port, Coast. Ocean Eng.*, 112: 460-465.
- Kirby, J.T. and Dalrymple, R.A., 1983. A parabolic equation for the combined refraction-diffraction of Stokes waves by mildly varying topography. *J. Fluid Mech.*, 136: 453-466.
- Kirby, J.T. and Dalrymple, R.A., 1984. Verification of a parabolic equation for propagation of weakly-nonlinear waves. *Coastal Eng.*, 8: 219-232.
- Kirby, J.T. and Dalrymple, R.A., 1986. An approximate model for nonlinear dispersion in monochromatic wave models. *Coastal Eng.*, 9: 545-561.
- Morris, J.L., 1983. *Computational Methods in Elementary Numerical Analysis*. John Wiley and Sons, New York, N.Y., 410 pp.
- Radder, A.C., 1979. On the parabolic equation method for water waves. *J. Fluid Mech.*, 95: 159-176.
- Tappert, F.D., 1977. The parabolic approximation method. In: J.B. Keller and J.S. Papadakis (Editors), *Wave Propagation and Underwater Sound*. Lecture Notes in Physics 70, Springer-Verlag, Berlin - Heidelberg, pp. 224.